Structural evolution in Au- and Pd-based metallic glass forming liquids and the case for improved molecular dynamics force fields

Cite as: J. Chem. Phys. **157**, 194501 (2022); https://doi.org/10.1063/5.0123907 Submitted: 01 September 2022 • Accepted: 18 October 2022 • Published Online: 15 November 2022

🗓 F. Z. Chen, K. Ruhland, C. Umland, et al.







ARTICLES YOU MAY BE INTERESTED IN

Experimental determination of the temperature-dependent Van Hove function in a $Zr_{80}Pt_{20}$ liquid

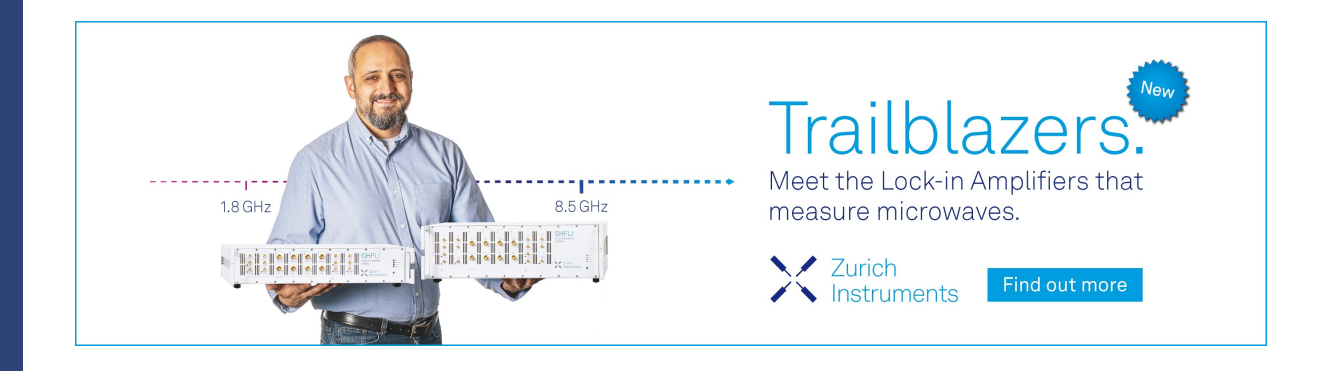
The Journal of Chemical Physics 152, 074506 (2020); https://doi.org/10.1063/1.5144256

Breakdown of the Stokes-Einstein relationship and rapid structural ordering in CuZrAl metallic glass-forming liquids

The Journal of Chemical Physics 155, 104501 (2021); https://doi.org/10.1063/5.0062724

Manifestations of static and dynamic heterogeneity in single molecule translational measurements in glassy systems

The Journal of Chemical Physics 157, 184506 (2022); https://doi.org/10.1063/5.0118892





Structural evolution in Au- and Pd-based metallic glass forming liquids and the case for improved molecular dynamics force fields

Cite as: J. Chem. Phys. 157, 194501 (2022); doi: 10.1063/5.0123907 Submitted: 1 September 2022 • Accepted: 18 October 2022 • Published Online: 15 November 2022







F. Z. Chen,¹ (D) K. Ruhland,² C. Umland,² S. M. Bertrand,² (D) A. J. Vogt,³ (D) K. F. Kelton,^{1,3} (D) and N. A. Mauro^{2,a)} (D)

AFFILIATIONS

- ¹ Institute of Materials Science and Engineering, Washington University, St. Louis, Missouri 63130, USA
- ²Department of Physics, St. Norbert College, De Pere, Wisconsin 54115, USA
- ³Department of Physics, Washington University, St. Louis, Missouri 63130, USA

ABSTRACT

The results of a combined experimental and computational investigation of the structural evolution of $Au_{81}Si_{19}$, $Pd_{82}Si_{18}$, and $Pd_{77}Cu_6Si_{17}$ metallic glass forming liquids are presented. Electrostatically levitated metallic liquids are prepared, and synchrotron x-ray scattering studies are combined with embedded atom method molecular dynamics simulations to probe the distribution of relevant structural units. Metal-metalloid based metallic glass forming systems are an extremely important class of materials with varied glass forming ability and mechanical processibility. High quality experimental x-ray scattering data are in poor agreement with the data from the molecular dynamics simulations, demonstrating the need for improved interatomic potentials. The first peak in the x-ray static structure factor in $Pd_{77}Cu_6Si_{17}$ displays evidence for a Curie-Weiss type behavior but also a peak in the effective Curie temperature. A proposed order parameter distinguishing glass forming ability, $1/(S(T, q_1) - 1)$, shows a peak in the effective Curie temperature near a crossover temperature established by the behavior of the viscosity, T_A .

Published under an exclusive license by AIP Publishing. https://doi.org/10.1063/5.0123907

I. INTRODUCTION

Alloys containing the metalloid-silicon pairing constitute an important family of metallic glass formers. The Au–Si eutectic alloy was identified nearly seventy years ago as the first glass forming composition. Despite the low melting temperature of the Au₈₁Si₁₉ eutectic composition, it has notoriously poor glass forming ability (GFA). It has been speculated that an incompatibility between the liquid and crystalline structures aids the eutectic depth, but it is not clear why that incompatibility does not improve GFA. Understanding the structural evolution of the Au–Si eutectic alloy is important since it is the base system for other Au-based alloys that have much improved GFA. At the same time, Pd–Si has been investigated for its improved GFA⁵ relative to Au–Si, forming the basis for its own family of bulk metallic glasses (BMGs). During the cooling process, the structure in the liquid state, especially under the

undercooled condition, changes considerably, 7-9 and the details of the structural evolution of the liquid has influence on subsequent phase formation. However, it has been a persistent challenge to quantify and describe the structures of undercooled metallic liquids in useful ways. This is made all the more important as Pd–Si BMGs possess unique mechanical properties. 10 The connection between GFA and structural evolution in the liquids continues to be poorly understood; however, there has been speculation about the most relevant structural features present in the liquids and their evolution with temperature. 11,12

The $Pd_{82}Si_{18}$ eutectic is a solute-lean system, and evidence suggests that each Si atom is surrounded in the nearest neighbor shell by Pd atoms only, ¹³ leading to solute–solute avoidance. This is a common phenomenon observed in other metallic glass forming families. ^{14,15} In Si-centered nearest neighbor clusters, the most probable CNs lie either at 9 or 10, whereas the Pd-centered clusters

a) Author to whom correspondence should be addressed: nicholas.mauro@snc.edu

are most frequently observed to have 12 or 13 neighbors but with a broad distribution. ¹⁶ In Pd₈₂Si₁₈, the tri-capped trigonal prisms with Voronoi Indices (VI)¹⁷ (0, 3, 6, 0) and (0, 2, 8, 0) are prevalent in the liquid, becoming more prevalent as the liquid is cooled into the glassy state. 7,16 Icosahedral clusters exist in Pd₈₂Si₁₈ but occur with low prevalence, 16 even in the glass. However, it remains unclear how icosahedral-like clusters¹⁸ related to the perfect icosahedra Voronoi index (0,0,12,0) are connected with GFA. This is further complicated because the Voronoi tessellation process does not distinguish slight distortions in one index that might be structurally relevant. With the suggestion that the formation of trigonal prisms or other "glass forming motifs" (Pd-centered Z13 and Si-centered Z9-like and mixed-ICO-cube clusters with five-fold local symmetry)¹⁹ is the key to glass formation in metal-metalloid systems, it is critical to reassess the validity of the potentials used in computer simulations against all available experimental structural data. It has been shown that the populations of trigonal prisms and, more importantly, prism clusters increase as the liquid is supercooled in computational studies. 20,21 These results depend significantly on the quality of the potentials used in the simulations.

We assess the quality of the Au-Si and Pd-Si potentials available by comparing the structures obtained from molecular dynamics (MD) simulations with the best x-ray scattering data available for Au- and Pd-based metallic glass forming liquids. In this work, we present a combination of experimental data and MD simulation results and structural analysis in Au₈₁Si₁₉, Pd₈₂Si₁₈, and Pd₇₇Cu₆Si₁₇ liquids. To our knowledge, this is the first examination of the Au-Si liquid structure from an experimental perspective, and while Pd-Si and Pd-Cu-Si structures have been generated using ab initio simulations, the embedded atom method (EAM) potentials and angular dependent potentials (ADP) have not been carefully examined and validated through systematic comparison with experimental structural data. Here, we compare the MD predictions for the structure, characterized by the radial distribution functions and structure factors, with experimental measurements of these quantities in the eutectic Au-Si and Pd-Si compositions. We find that the correspondence between the experimental data and the EAM results is poor in Pd₈₂Si₁₈ and extremely poor in Au₈₁Si₁₉. The importance of refining the EAM potentials in these metal-metalloid systems is further reinforced as a proposed order parameter for distinguishing glass forming ability, shows a peak in its effective Curie temperature near a crossover temperature established by the behavior of the viscosity, T_A . In order to understand the evolution of dominant structures in these systems, the EAM potentials require refinement based on our experimental scattering data.

II. EXPERIMENTAL

Master ingots for all compositions were prepared by arcmelting high-purity Pd (99.99 at.%), Cu (99.995 at.%), Au (99.9 at.%), and Si (99.9999 at.%) to produce ~1 g ingots of Au₈₁Si₁₉, Pd₈₂Si₁₈, and Pd₇₇Cu₆Si₁₇. A Ti−Zr getter located close to the sample was melted prior to arc-melting the master ingots as an oxygen getter. The master ingots were melted three times to ensure that the samples were homogeneous. Potential mass loss was measured due to the arc-melting process and was negligible for all samples (less than 0.1%). The master ingots were used as source material to create spherical samples (2.25−2.60 mm diameter) that were

processed in the Washington University Beamline Electrostatic Levitation (WU-BESL) facility. The WU-BESL is optimized for x-ray diffraction studies of levitated, containerlessly processed, liquids in a high-vacuum environment (10^{-8} – 10^{-7} Torr). The $Pd_{82}Si_{18}$ samples prepared for study in the WU-BESL were first fluxed in B_2O_3 to improve processibility and supercooling. The WU-BESL was installed at the D-station at Sector 6 of the Advanced Photon Source (APS). To minimize the effect of the beryllium x-ray entrance window on the scattering signal, external lead and internal tungsten shielding remove the scattering of the direct beam from that window. In addition, a beamstop is installed just downstream (outside of the chamber) of the beryllium exit window, which captures the scattering of the direct beam from that window but produces a slight fluorescence signal at very low-q.

The levitated samples were processed using a 50 W maximum continuous power output, fiber coupled diode laser operating at a wavelength of 980 nm. A Process Sensors Metis MI18 single color pyrometer operating at a wavelength of 1.89 µm was used to measure the levitated samples at lower temperatures (160-800 °C), and a Metis MQ22 two-color ratio pyrometer operating at 1.40 and 1.65 µm wavelengths was used for the high temperature measurements (600-2300 °C). The emissivities of the various samples were calibrated by matching the end of the melt plateau (corresponding to the eutectic temperature, $T_{\rm S}$, in the temperature vs time curve measured on heating in WU-BESL) to the largest endothermic signature measured in a differential thermal analyzer (DTA; Labsys DTA/DSC, Setaram).²⁴ The temperature was correlated with noncontact measurements of the volume, made using the shadow method^{25,26} with a PixeLINK PL-B74IG CMOS camera and a 455 nm collimated microscope light-emitting diode (LED). The relative precision of the measured density data was ~0.3% over the temperature range studied with an absolute accuracy of $\sim 0.5\%$ for $Pd_{82}Si_{18}$ and $Pd_{77}Cu_7Si_{16}$ and $\sim 1.5\%$ for $Au_{81}Si_{19}$. A more detailed discussion of the machine vision volume measurement algorithm and experimental implementation can be found

The diffraction studies were made in a transmission geometry using high-energy x rays ($E=130~{\rm keV}, \lambda=0.094~{\rm Å}$). Scattering data were obtained to a momentum transfer, q, maximum of 17 Å $^{-1}$, at a sampling rate of 1 Hz (isothermal) and 2 Hz (slow, controlled cooling) using a General Electric (GE) Revolution 41-RT amorphous Si flat-panel x-ray detector. A diffraction pattern from a NIST Si standard was used to calibrate the detector position, and orientation and bad pixels were removed. After applying a pixel efficiency gain map, images were corrected for oblique incidence, absorption, multiple scattering, fluorescence, polarization, sample geometry, Compton scattering and container scattering contributions using in-house analysis packages written in LabVIEW $^{\rm TM}$. Data were collected either in a series of 10 s isothermal scattering measurements in a controlled cooling mode by modulating the heating laser power. The static structure factor was calculated using

$$S(q) = \frac{I(q) - \sum_{i=1}^{n} c_i |f_i(q)|^2}{\left|\sum_{i=1}^{n} c_i f_i(q)\right|^2} + 1,$$
 (1)

where I(q) is the measured intensity, c_i is the atomic fraction of each elemental species, and $f_i(q)$ is the q-dependent atomic form factor for each element. Given the common assumption of isotropic

scattering and a homogeneous sample, the total pair-distribution function, g(r), was computed from a Fourier transform of the structure factor,

$$g(r) - 1 = \frac{1}{4\pi\rho_0} \frac{2}{\pi} \int (S(q) - 1) \frac{\sin(qr)}{qr} q^2 dq,$$
 (2)

where ρ_0 is the number density.

Incomplete accounting for secondary scattering is one of the primary causes of incorrect scaling of the static structure factor. In practice, it is impossible to properly model the secondary scattering without knowing the precise configuration of the scattering environment. A procedure developed by Peterson *et al.*²⁷ and widely adopted in the neutron and x-ray scattering community was used to slightly adjust the scaling in the structure factor to reduce Fourier transformation truncation ripples. In this process, ΔG_{low} [Eq. (4)], which quantifies the magnitude of ripples in G(r) below the hardsphere cutoff, is minimized, and then, the structure factor is rescaled [Eq. (4)] until the experimentally measured number density $\rho_{\rm exp}$ matched $\rho_{\rm fit}$ as closely as possible,

$$\Delta G_{low} = \frac{\int_{0}^{r_{low}} \left(r G(r) + 4\pi r^2 \rho_{fit} \right)^2 dr}{\int_{0}^{r_{low}} \left(4\pi r^2 \rho_{fit} \right)^2 dr},$$
 (3)

$$S'(q) = \alpha S(q) + (1 - \alpha). \tag{4}$$

The difference between the experimental and fit number densities was found to be about 0.5% for Au–Si and Pd–Si and about 1.5% for Pd–Cu–Si. This treatment has been validated in x-ray and neutron diffraction experiments conducted at the same temperature from two separate x-ray scattering studies. The positions and magnitudes of the first peaks in S(q) were refined by fitting a cubic spline to the peak using in-house programs written in Python. The uncertainties in the structure factors presented were estimated by considering perturbations from independent sources of error (including statistical uncertainties) following the method described by Hammersley and from the confidence intervals of fitted correction factors. The precision of the peak heights in S(q) presented was between 0.5% and 1.2% for the data collected.

III. MOLECULAR DYNAMICS SIMULATIONS

Molecular dynamics (MD) simulations were made for the $Pd_{82}Si_{18}$ and $Au_{81}Si_{19}$ metallic liquids. The large-scale atomic/molecular massively parallel simulator (LAMMPS) was chosen for the MD studies, which were made using the NSF computing resources in the Extreme Science and Engineering Discovery Environment (XSEDE).³¹ The embedded atom method (EAM) potential ^{32,33} and the angular dependent potential (ADP) ³⁴ were used to describe the atomic interactions for the $Pd_{82}Si_{18}$ and the $Au_{81}Si_{19}$ metallic liquids, respectively. The $Pd_{82}Si_{18}$ and $Au_{81}Si_{19}$ metallic liquids were made by first randomly arranging 32 000 atoms and 30 000 atoms, respectively, at 2000 K and then relaxing the ensembles for 1 ns to reach equilibrium. The ensembles were then cooled at a constant rate (10 K/ps) and subsequently equilibrated for 20 ns at the target temperature for further analysis.

We confirmed that the ensembles had thermally equilibrated by comparing various quench rates and ensuring that the structure factors and pair-distribution functions converged (shown in the supplementary material, Figs. 1–4). All of the MD simulations were made under NPT (isobaric–isothermal) conditions, and periodic boundary conditions were assumed.

IV. RESULTS AND DISCUSSION

A. Structure factor and pair correlation function results for Au-Si and Pd-Si

The total structure factors, S(q), were calculated from measured high-energy x-ray diffraction data for $Au_{81}Si_{19}$ and $Pd_{82}Si_{18}$ metallic liquids for several 100 degrees around their respective liquidus temperatures (Fig. 1). Both metals display a main peak, $S(q_1)$, which increases upon cooling, indicating an increasing coherence length for the structures in the liquid—a universal feature for metallic liquids. Furthermore, and also consistent with previous investigations, the peak position, q_1 , shifts to higher-q with decreasing temperature, consistent with an increasing atomic density. The structure factors for the Pd-Si alloy studied also develop a distinct shoulder on the second peak as the temperature is lowered—a feature missing in the Au-Si metallic liquid. All of the S(q)s oscillate around unity owing to the superior sample environment. Electrostatic levitation removes the need for capillaries and other sample environments that corrupt the background corrections necessary to produce clean and physical structure factors. This is particularly relevant as we compare the experimentally determined x-ray data to the MD

Molecular dynamics simulations are powerful tools for studying the details of the three-dimensional structures that are present in metallic liquids. However, the accuracy of the atomic potentials used for the simulations must be validated by comparing MD predictions with experimental data. Here, we compare the experimental and MD generated S(q)s. The partial pair-distribution functions (PPDFs), $g_{\alpha\beta}(r)$, were calculated directly from the MD simulation ensemble as

$$g_{\alpha\beta}(r) = \frac{1}{4\pi r^2 N \rho_o} \sum_{i=1}^{N} \sum_{j=1 \pm i}^{N} \langle (r - r_{ij}) \rangle,$$
 (5)

where N is the number of atoms and r_{ij} is the distance between the ith and the jth atoms. At each temperature, the simulations were equilibrated for 20 ns before summing the PPDFs together to obtain the g(r)s. Furthermore, once the PPDFs were calculated, the associated partial structure factors (PSFs) were calculated according to

$$S_{\alpha\beta}(q) = 1 + 4\pi\rho_0 \int_0^\infty r^2 g_{\alpha\beta}(r) \frac{\sin(qr)}{qr} dr.$$
 (6)

To compare with the experimental x-ray scattering results, the total S(q) was calculated by summing the PSFs with the appropriate x-ray Faber–Ziman weighting factors.³⁵ Figure 2 shows a comparison between the experimental and MD calculated S(q)s for $Pd_{82}Si_{18}$ and $Au_{81}Si_{19}$. Prior to the structural calculation, all the samples were

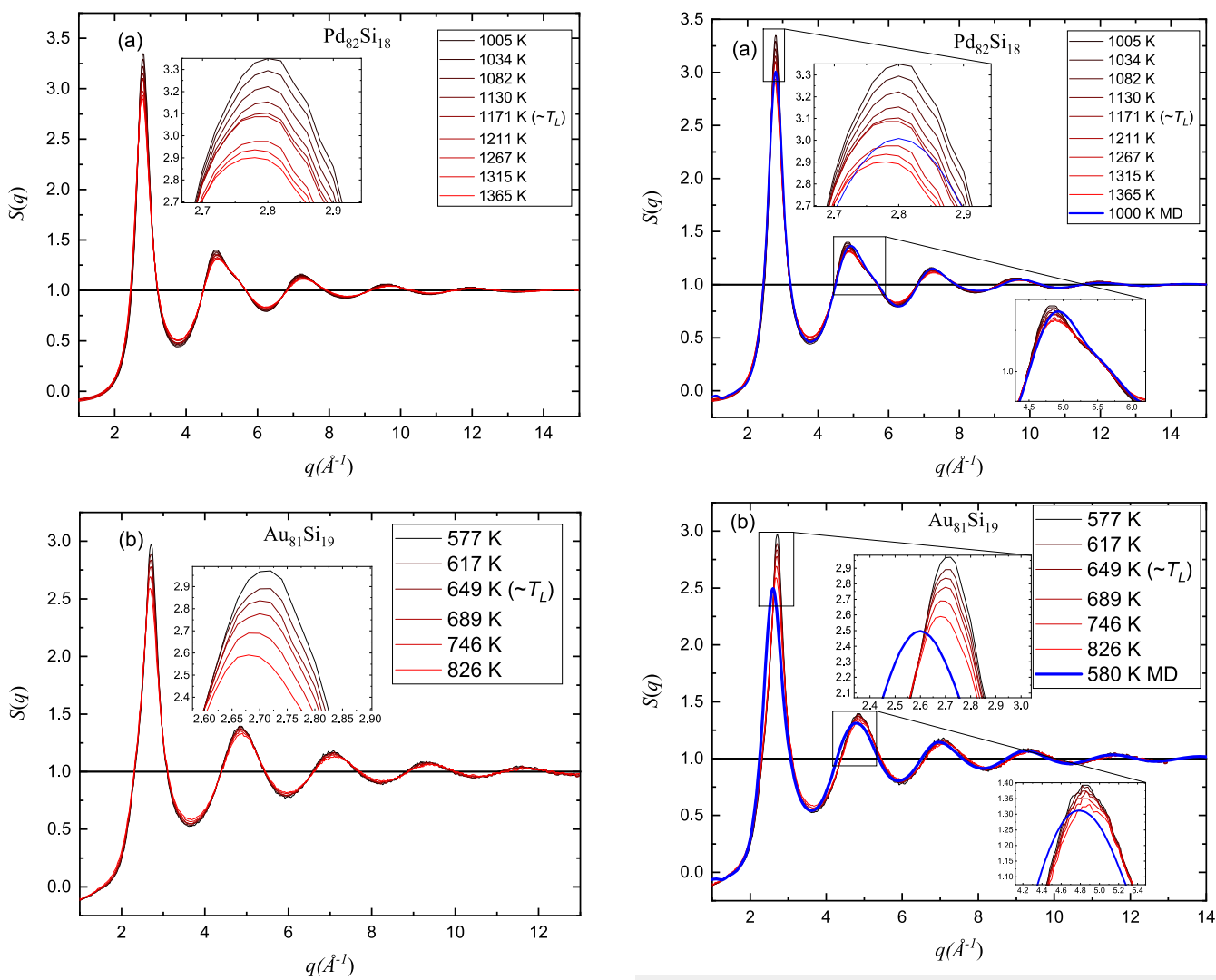


FIG. 1. Experimentally determined static structure factors for (a) $Pd_{82}Si_{18}$ and (b) $Au_{81}Si_{19}$. The measured structure factors demonstrate a main peak (shown in the inset) that increases in intensity and shifts to higher-q with decreasing temperature, consistent with an increasing atomic density. A distinct shoulder on the second peak also develops as the temperature is lowered for $Pd_{82}Si_{18}$, a feature that is not present in the Au–Si liquids. The data taken closest to the liquidus temperatures ($T_L = 1081$ and 632 K for $Pd_{82}Si_{18}$ and $Au_{81}Si_{19}$, respectively) are indicated for reference.

FIG. 2. Comparison between the experimental structure factors for $Pd_{82}Si_{18}$ and $Au_{81}Si_{19}$ with the lowest temperature obtained from the MD simulation. (a) The MD structure factor for $Pd_{82}Si_{18}$ at 1000 K is inconsistent with the experimental data. The main peak positions match, but the peak height is low by nearly 11%. Furthermore, the shoulder on the second peak shown in the lower inset deviates considerably. (b) The correspondence between the MD structure factor with the corresponding x-ray structure factor for Au-Si at 580 K is very poor. The main peak position deviates by ~6% while the peak height deviates by almost 17%, suggesting major flaws in the force field. The data taken closest to the liquidus temperatures ($T_L=1081$ and 632 K for $Pd_{82}Si_{18}$ and $Au_{81}Si_{19}$, respectively) are indicated for reference.

relaxed at the target temperature for 20 ns to reach equilibrium before the analysis. For clarity, the MD results are shown for only the lowest temperature studied in the simulation of each liquid. As can be seen, there is substantial disagreement between the experimental and simulation results at the lowest temperature for both liquids; similar disparities are observed at all temperatures as are shown in the supplementary material (Figs. 5 and 6). The height of the first peak in the MD calculated S(q) at 1000 K is ~11% lower than the experimental value in the $Pd_{82}Si_{18}$ liquid [Fig. 2(a)] although

the peak positions are similar. Furthermore, the appearance of two sub-peaks in the second peak in S(q) found in the experimental data at lower temperatures is not reproduced accurately in the MD calculated S(q) [see the lower inset in Fig. 2(a)]. This latter point is particularly concerning since this feature is sensitive to developing local order 14,15,28,36 in the liquid, which is not reproduced in the MD calculations. The differences between the MD and experimental data for S(q) at the lowest temperature studied by MD (580 K) in

TABLE I. Measured liquid density temperature dependency. The solidus temperatures, T_s , were obtained with DTA and are consistent with literature values where available. 37,38

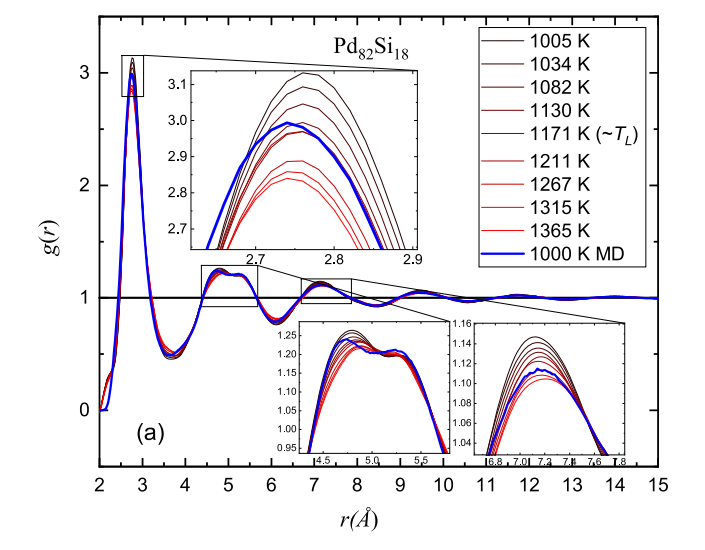
Composition	Solidus temperature, T_s (K)	Liquidus temperature, T_L (K)	Density, ρ , at T_L (g/cm ³)	$d\rho/dT (10^{-4} g/cm^3/k)$
Au ₈₁ Si ₁₉	632	632	15.58	-11.7
$Pd_{82}Si_{18}$	1081	1081	10.14	-7.52
$Pd_{77}Cu_6Si_{17} \\$	1013	1128	10.00	-7.24

the $Au_{81}Si_{19}$ liquid are even more striking [Fig. 2(b)]. The first peak positions differ by ~6% while the peak height is almost 17% lower than the experimental data at a corresponding temperature.

Similar differences between the experimental data and the results of the MD simulations are also found for the pair-distribution function, g(r). This function provides an average description of the liquid structure, giving the probability of finding a particle at a distance r from an average central atom, normalized to the average number density, and is obtained directly from the MD simulation [Eq. (5)]. The experimental value for g(r) is obtained from a Fourier transform of the experimental structure factor [Eq. (2)]. The densities needed were determined experimentally using the shadow method described earlier; they are presented in Table I.

As with S(q), the experimental values of g(r) for $Au_{81}Si_{19}$ and Pd₈₂Si₁₈ compare poorly at all temperature, and we show a comparison at the lowest temperature MD simulation (Fig. 3). Comparisons at other temperatures also show poor agreement, as shown in the supplementary material (Figs. 7 and 8). In Fig. 3(a), the intensity of the first peak in the MD generated g(r) for Pd₈₂Si₁₈ at 1000 K is ~5% less than the experimental value. The splitting in the second peak is also inconsistent between the MD and experimental data. The correspondence between the MD pair-distribution function and the experimental one is even worse for the Au₈₁Si₁₉ liquid, as shown in Fig. 3(b). Again, the magnitude of the first peak in the MD generated g(r) at 580 K is much smaller than the experimental value at 577 K. The peak positions for the second and higher coordination shells are shifted to larger values of r than the experimental data, and while the second peak has the beginnings of an asymmetry in the MD data, it is much less than in the experimental data. The deviations extend to the bulk density as well, where the MD value (14.3 g/cm³) is almost 7% smaller than the experimental value—a statistically significant difference. The differences between the MD and experimental data in the second peak of g(r) are particularly troubling. There is a considerable body of literature attempting to interpret the evolution of the splitting of the second peak.³⁹ The fact that it does not occur in the MD generated structures to the same degree as from the x-ray data indicates that the MD structure is more homogeneous than the experimental one, as will be discussed in more detail in Sec. IV B.

A critical point from these differences between the experimental and the MD calculated values for S(q) and g(r) is that the local structures in the liquid are not well represented by the potentials used. This is discussed further in Sec. IV B, showing differences in the local structures obtained from the MD simulations discussed here and from ab initio calculations. The differences with the experimental data and the results of ab initio studies clearly indicate that the potentials for both the $Au_{81}Si_{19}$ and $Pd_{82}Si_{18}$ liquids need to be further refined.



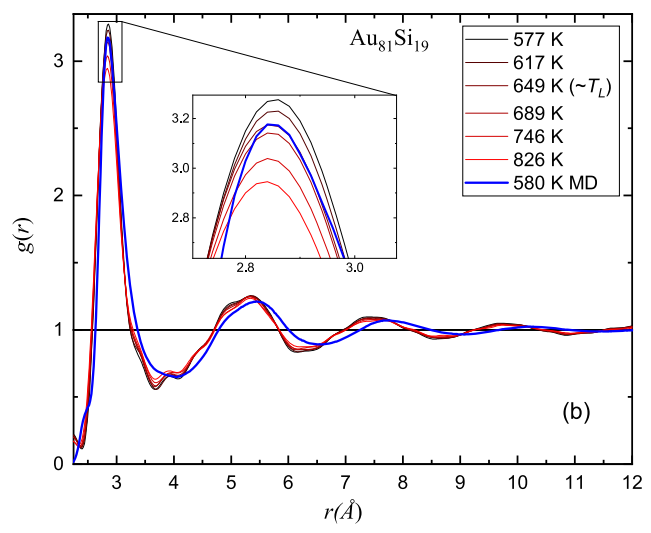


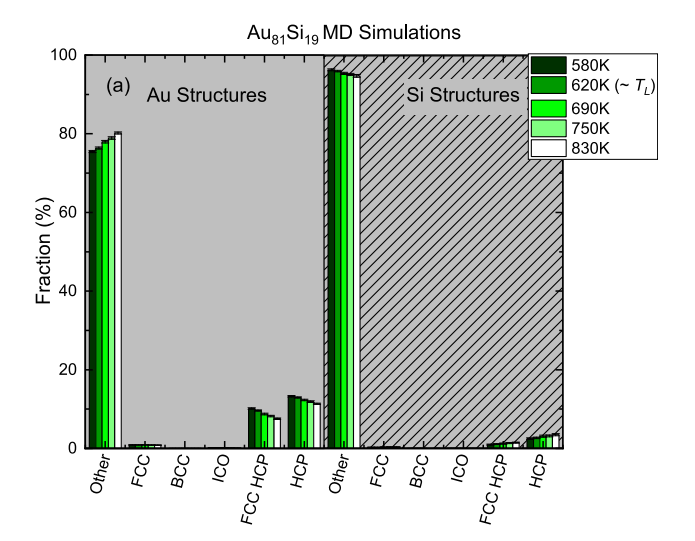
FIG. 3. Comparison between the experimentally determined pair-distribution functions for $Au_{81}Si_{19}$ and $Pd_{82}Si_{18}$ with the lowest temperature obtained from the MD simulation. (a) The MD pair-distribution for $Pd_{82}Si_{18}$ at 1000 K is inconsistent with the experimental data. The inconsistencies between the main peaks are obvious, but the important splitting in the second peak is quantitatively inconsistent, suggesting simulated structures that deviate considerably in the nearest and second-nearest neighbor distance. (b) The correspondence between the MD pair-distribution function with the corresponding x-ray function for Au—Si at 580 K is very poor, particularly in the second and higher coordination shell *r*-range. The data taken closest to the liquidus temperatures ($T_L = 1081$ and 632 K for $Pd_{82}Si_{18}$ and $Au_{81}Si_{19}$, respectively) are indicated for reference.

B. Molecular dynamics Voronoi analysis

In order to effectively characterize a given liquid structure and extract the important structural characteristics of glass formation, many topological methods have been proposed including the Honeycutt-Anderson common neighbor analysis,40 the bond orientation order parameter,⁴¹ and the Voronoi tessellation method.¹⁷ The Voronoi tessellation method allows one to decompose the structures present in the MD simulations quantitatively based on polyhedral order. In this method, the perpendicular bisecting plane between each pair of atoms is constructed, weighted according to the atomic size. The convex polyhedron around each central atom is then characterized by its "Voronoi index," $\langle n_3, n_4, n_5, \dots, n_i, \dots \rangle$, where n_i is the number of *i*-sided polygons of the enclosing polyhedron. In this way, the local order around each atom can be characterized with a distinct, natural topology. In our analysis, polyhedral faces that constitute less than 1% of the total face area are removed and the Voronoi index without that small face is indexed. In this way, the Voronoi index characterizing each atom more accurately reflects the nearest neighbor atomic ordering. Following the procedure outlined above, MD simulations of liquid Au₈₁Si₁₉ and Pd82Si18 were prepared over several hundred degrees Kelvin near the liquid temperatures. At each temperature, 3000 simulations were prepared with each separated by 10 fs. A configuration was sampled every picosecond, and a complete Voronoi tessellation analysis was completed using the OVITOTM Open Visualization Tool, 42 allowing the generation of descriptive statistics on the structures present in each simulation.

A common approach to characterizing the Voronoi structures is to group them into close-packed cubic (FCC and HCP), bodycentered cubic (BCC), icosahedral (ICO), and other structures.⁴² In Fig. 4, we present such an analysis on both the Au-Si and Pd-Si MD simulations at each temperature for which there is also experimental data. It is important to stress that any such analysis relies on the force fields generating the structures being physical and that there exists a high degree of correspondence between the experimental x-ray data [S(q)] and g(r) in this case and the associated MD data. For both systems, the most prevalent structure is non-cubic and imperfect icosahedral. The Au-based alloy demonstrates a tendency for non-cubic structures relative to the Pd-based alloy, but given the poor correspondence between the x-ray and MD structure factors and pair-distribution functions, this cannot be considered conclusive. Perhaps, the most useful element of this very broad analysis is the evidence that the simulations have equilibrated. By comparing the fraction of FCC, BCC, ICO, etc., order present, no statistically significant deviations from the average presented in Fig. 4 were observed over the course of the isothermal simulations.

Previous investigations⁴³ used first-principles MD simulations to study the local structures in $Pd_{82}Si_{18}$. A Voronoi analysis of those simulation results found a high frequency of Pd (0,0,12,0,0), (0,2,8,2,0), (0,3,6,3,0), (0,1,10,2,0), (0,3,6,4,0), and (0,2,8,4,0) structures, constituting of almost 40% of all Pd-centered structures, and a high frequency of Si (0,3,6,0,0), (0,2,8,0,0), (0,3,6,1,0), (1,2,5,2,0) and (0,2,8,1,0) structures, constituting of almost 50% of all Si-centered structures. We carried out a Voronoi analysis of these same structures in $Au_{81}Si_{19}$ and $Pd_{82}Si_{18}$ (Fig. 5). Generally speaking, the distribution of Voronoi structures present in Au-Si liquids [Fig. 5(a)] is extremely broad.



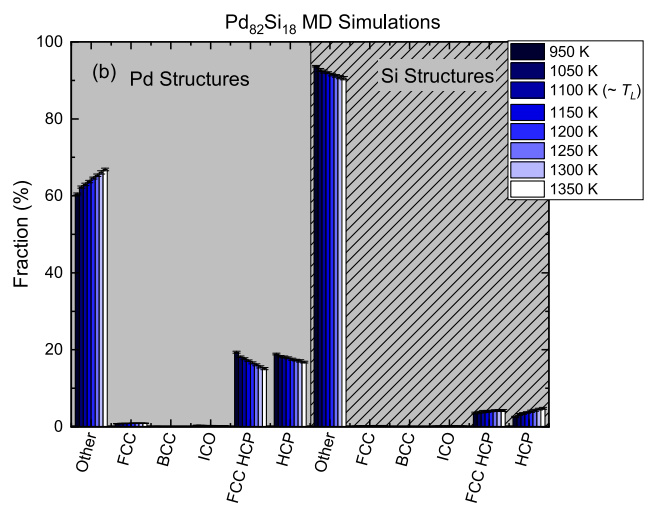
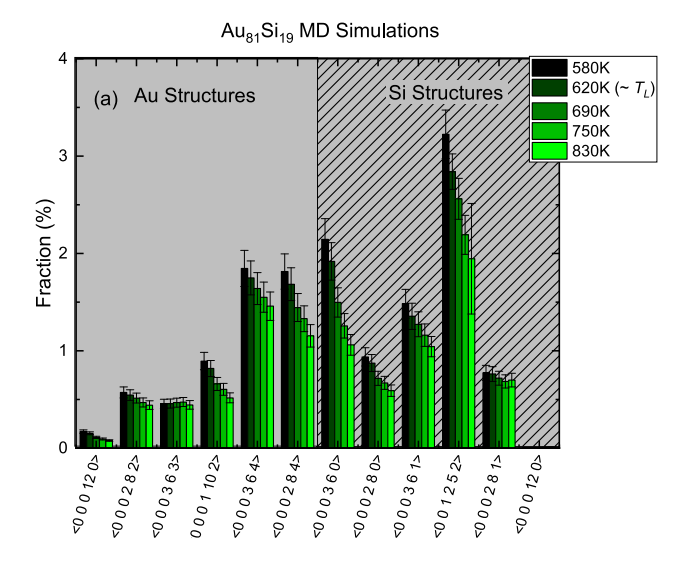


FIG. 4. Voronoi tessellation analysis of Au–Si and Pd–Si liquids grouping the structures by type. The uncertainties included on the graphs come from the standard deviation of the configurations sampled. For both systems, the most prevalent structure is non-cubic and imperfect icosahedral. The Au-based alloy demonstrates a tendency for non-cubic structures relative to the Pd-based alloy, but given the poor correspondence between the x-ray and MD structure factors and pair-distribution functions, this cannot be considered conclusive. The data taken closest to the liquidus temperatures ($T_L = 1081$ and 632 K for $Pd_{82}Si_{18}$ and $Au_{81}Si_{19}$, respectively) are indicated for reference.

No single index exceeds 2.1% of the total structures, regardless of atomic species and the distribution narrows as the temperature decreases; the perfect icosahedral structure, $\langle 0,0,12,0,0 \rangle$, has a very sparse frequency in all simulations. Interestingly, the $\langle 1,2,5,2,0 \rangle$ Si structure is present with a substantially higher frequency than in the Pd–Si alloy in this and previous⁴³ studies.

It is interesting that the Si structures in $Pd_{82}Si_{18}$ appear to have some similar characteristics to previous studies. At 950 K, the most abundant structures are $\langle 0, 2, 8, 0, 0 \rangle$, $\langle 0, 3, 6, 0, 0 \rangle$, $\langle 0, 2, 8, 1, 0 \rangle$, and $\langle 0, 3, 6, 1, 0 \rangle$, which are similar to, but not entirely consistent with,



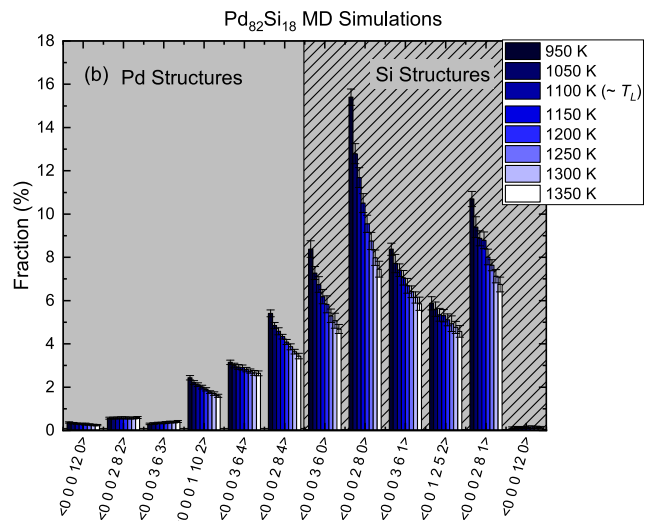


FIG. 5. Voronoi tessellation distribution of Au–Si and Pd–Si liquids at different temperatures. The data taken closest to the liquidus temperatures ($T_L=1081$ and 632 K for $Pd_{82}Si_{18}$ and $Au_{81}Si_{19}$, respectively) are indicated for reference.

previous studies. We observe even more substantial inconsistencies between our Pd structures and previous work. We observe a much broader distribution of Pd Voronoi structures. Where previous studies found a high prevalence of $\langle 0,1,10,2,0 \rangle$ and $\langle 0,3,6,4,0 \rangle$, both exceeding 10% around 950 K, we observe only a quarter of those values. These results, combined with the poor correspondence between the experimental and MD simulation structure factors and pair-distribution function for both systems, suggest that that the potentials used for the MD simulations require refinement. Many computational and experimental studies have shown that the pure icosahedral structure $\langle 0,0,12,0,0 \rangle$ usually does not have a high concentration in many metallic glass forming compositions. The Voronoi tessellation method is one of the most widely used

TABLE II. Voronoi structures grouped into "primary" and "secondary" categories.

Primary structures	Secondary structures		
(0,0,12,0,0) (0,1,10,2,0) (0,2,8,1,0) (0,2,8,2,0)	(0,4,4,5,0) (0,1,10,3,0) (0,3,6,0,0) (0,2,8,4,0) (0,2,8,3,0) (0,4,4,2,0) (0,4,4,4,0)	\(\langle 0, 2, 8, 0, 0 \rangle \) \(\langle 0, 3, 6, 1, 0 \rangle \) \(\langle 0, 3, 6, 4, 0 \rangle \) \(\langle 0, 3, 6, 2, 0 \rangle \) \(\langle 0, 4, 4, 3, 0 \rangle \) \(\langle 0, 3, 6, 3, 0 \rangle \)	

for characterizing icosahedral-like order. 7,17,47,48 A scheme has been proposed for identifying and distinguishing "quasi-icosahedral" clusters relevant for metallic glass formation. 18 The projection method was used in this work to connect the perfect icosahedral Voronoi index $\langle 0,0,12,0,0\rangle$ to three other full-icosahedral clusters: $\langle 0,1,10,2,0\rangle,\ \langle 0,2,8,1,0\rangle,\$ and $\langle 0,2,8,2,0\rangle.$ We refer to these as "primary structures." Furthermore, we combine structures related to these primary structures by simple deformations 18 into a grouping called "secondary structures." These structures have been identified in various studies as important, prevalent, and have been linked to glass forming ability in one way or another. The Voronoi structures that we characterize as primary and secondary are summarized in Table II.

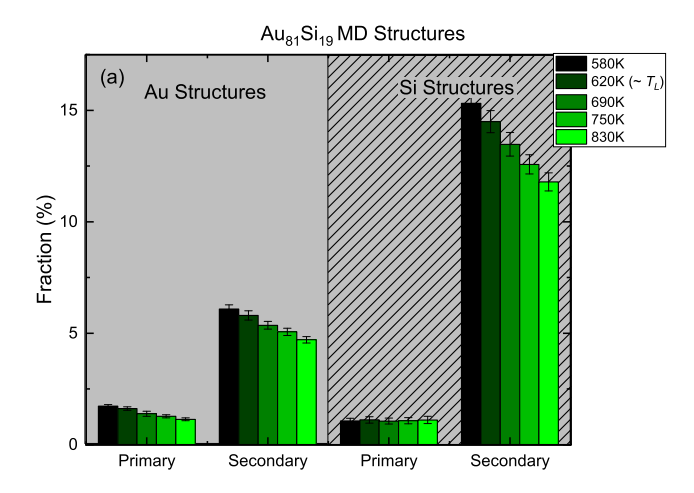
The Voronoi tessellation distribution of Au-Si and Pd-Si liquids at different temperatures, grouped into primary and secondary structures according to the scheme in Table II, is shown in Fig. 6. A value of these grouping schemes is improved statistics. The argument is made¹⁸ that these groupings gather topologically similar structures and that their evolution with temperature can be connected to glass forming ability, without suffering from the statistics of small numbers. As shown in Fig. 6(a), the groupings of structures into primary and secondary still only account for less than 12% of the total Si structures (and less than 6% of the Au structures) in the Au-Si, whereas Si structures in Pd-Si [Fig. 6(b)] are well represented in this group scheme. The rapid increase in secondary Si structures with decreasing temperature is consistent with Fig. 5(b) since (0, 2, 8, 0, 0), (0, 3, 6, 0, 0), and (0, 3, 6, 1, 0) are grouped in the secondary category. These results again show that the potentials used for Au-Si (in particular) and Pd-Si need refinement and the broad distribution of structures observed in Fig. 6 is further evidence for

C. Order parameter analysis

The order parameter

$$O(T) = 1/(S(q_1) - 1),$$
 (7)

where $S(q_1)$ is the height of the first peak of the static structure factor, is a possible differentiator of glass forming ability in metallic liquids. We have argued that this parameter could identify the structural signature of an accompanying dynamical transition. ⁴⁹ In the theoretical case of infinite ordering, corresponding to an infinite coherence length, the parameter O(T) goes to zero. We have previously argued that O(T) is related to the rapid increase in the



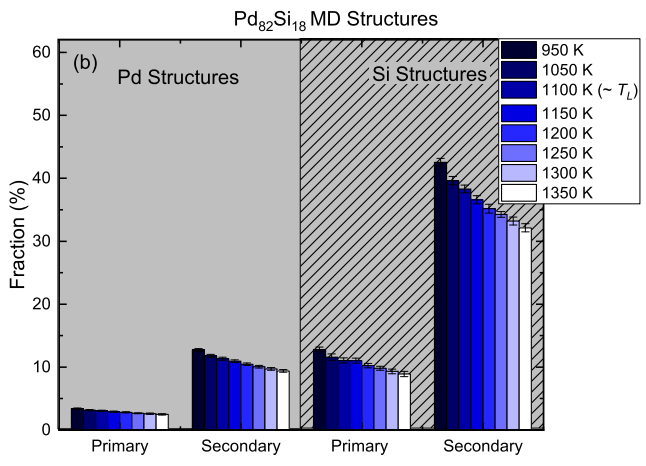
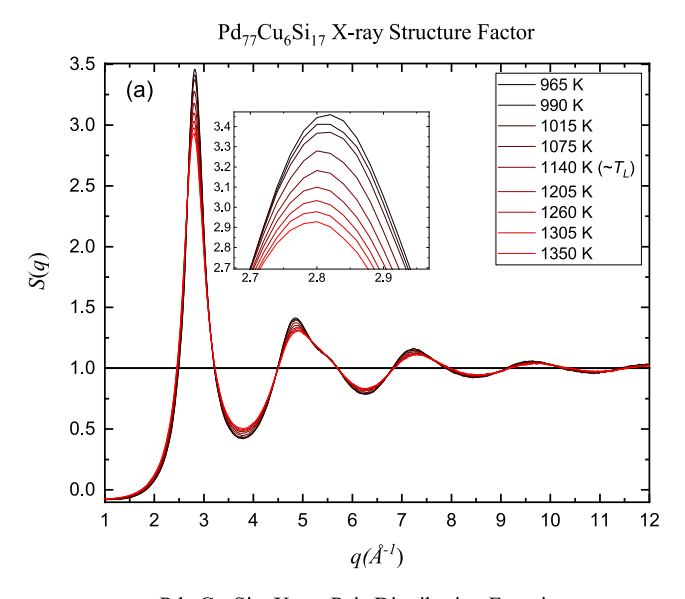


FIG. 6. Voronoi tessellation distribution of Au–Si and Pd–Si liquids at different temperatures grouped into primary and secondary structures according to the scheme in Table II. (a) The groupings of structures into primary and secondary still only account for less than 12% of total Si structures (less than 6% for Au structures). The increase in primary Si structures is within error and is likely not statistically significant. (b) Si structures in Pd–Si [Fig. 6(b)] are well represented in this group scheme, accounting for 32%–42% over the temperature range studied. The rapid increase in secondary Si structures (0,2,8,0,0), (0,3,6,0,0), and (0,3,6,1,0) are grouped in the secondary category. The data taken closest to the liquidus temperatures ($T_L = 1081$ and 632 K for $Pd_{82}Si_{18}$ and $Au_{81}Si_{19}$, respectively) are indicated for reference

liquid viscosity with decreasing temperature, reflecting the fragility of the liquid. Fragility correlates with glass forming ability, so differences in O(T) among liquids investigated might be expected; however, this order parameter has not been experimentally explored in multiple metallic glass forming systems. In largely theoretical investigations, the order parameter O(T) was shown to follow a Curie–Weiss law. The metallic glass forming liquid $Pd_{77}Cu_6Si_{17}$ has superior GFA compared to $Pd_{82}Si_{18}$ and provides an excellent opportunity to explore this order parameter. This system has attracted interest for its enhanced thermal stability but also the possibility that Cu-additions can induce structural changes in the

liquid that can be readily interpreted in terms of icosahedral ordering.⁵¹

We have investigated the structural evolution in the $Pd_{77}Cu_6Si_{17}$ liquid through high-energy x-ray diffraction studies. For these measurements, the high temperature liquid was allowed to cool slowly into the undercooled liquid state while diffraction images were collected at two frames per second (2 Hz) over a temperature range of 1350 down to 965 K. The static structure



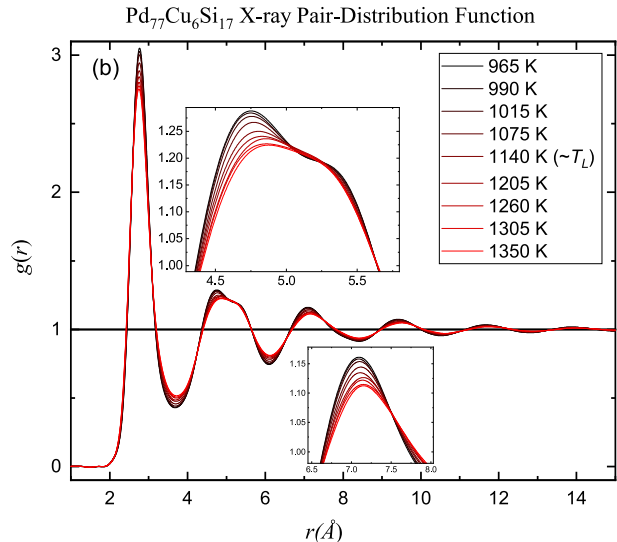
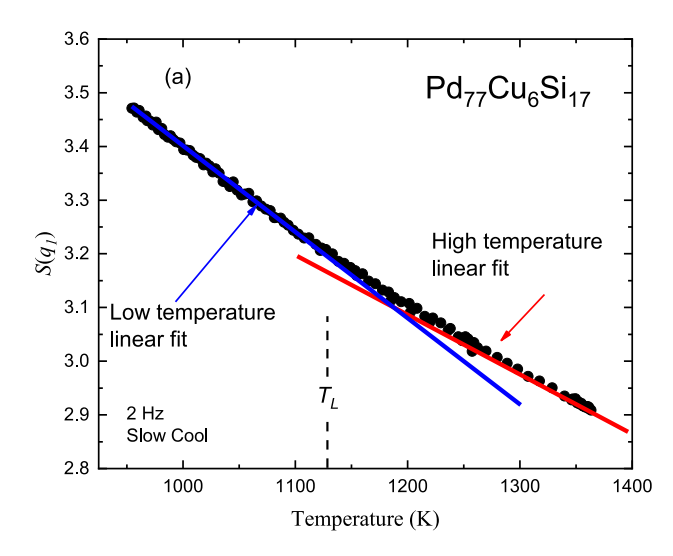


FIG. 7. Experimentally determined (a) static structure factors and (b) calculated pair-distribution functions for liquid $Pd_{77}Cu_6Si_{17}$. (a) The measured structure factors demonstrate a main peak (shown in the inset) that increases in intensity and shifts to higher-q with decreasing temperature, consistent with an increasing atomic density. A distinct shoulder on the second peak also develops as the temperature is lowered. (b) The calculated pair-distribution functions were calculated from Eq. (2). The data taken closest to the liquidus temperature ($T_L = 1128$ K) are indicated for reference.

factors and associated pair-distribution functions were calculated and are presented in Fig. 7. Due to the clean scattering environment in the BESL, these are quantitatively reliable and to our knowledge the highest quality data available on this system.

Furthermore, detailed analyses of the structural data provide tantalizing evidence that a structural signature of a cooperative dynamics may be present. As is illustrated in Fig. 8(a) for the $Pd_{77}Cu_6Si_{17}$ liquid, the evidence of structural ordering is present in the $S(q_1)$ and, subsequently, the behavior of the order parameter in Eq. (7). The evolution of the first peak in the structure factor is non-linear with an apparent crossover temperature between a "high



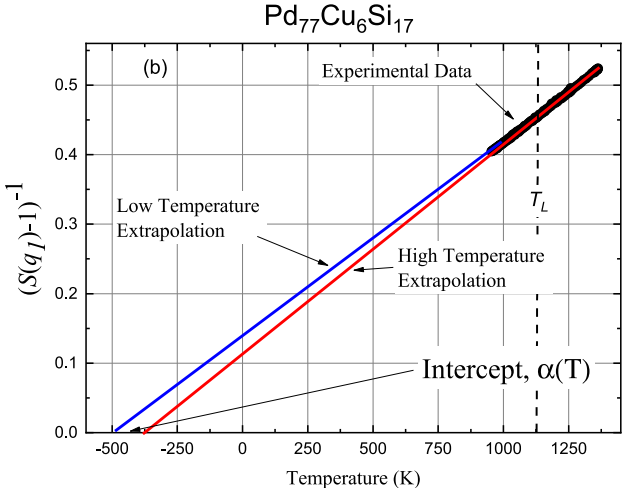


FIG. 8. (a) The first peak in the static structure factor as a function of temperature for liquid $Pd_{77}Cu_6Si_{17}$. Data were obtained from diffraction images collected at two frames per second (2 Hz). (b) Projection of the order parameter down to the temperature axis, showing the dependence on the temperature range of the data used. The intercept, $\alpha(T)$, is strongly temperature dependent, is observed to be non-monotonic, and provides a measure of an effective Curie temperature for the liquid at a particular liquid temperature, T. The liquidus temperature ($T_L = 1128 \text{ K}$) is shown for reference in each figure.

temperature" and a "low temperature" behavior. Similar crossovers or inflections have been observed in other metallic glass forming systems.²⁸

Our analysis of the behavior of the static structure factor, and thus the order parameter, is based on the fact that a Taylor expansion of a weakly exponential function can often display nearly linear behavior. We fit the first peak in the static structure factor to an exponential according to

$$S(q_1) - 1 = ae^{bT} + c (8)$$

using a weighted least squares regression. In Fig. 8(b), the intercept, $\alpha(T)$, of the projection of the order parameter is the effective Curie temperature. We find that, similar to how the temperature dependence of the viscosity defines the fragility of the liquid, the order parameter O(T) provides a measure of rates of structural ordering. Specially, the projection of the order parameter down to the temperature axis provides a measure of an effective Curie temperature.

Following a method presented by Chen *et al.*, ²⁸ it follows from Eq. (8) that the Curie temperature has an analytical form and can be simplified to

$$\alpha(T) = T + 1/b + c/abe^{bT}.$$
 (9)

Taking the temperature derivative of Eq. (9) shows that $\alpha(T)$ does not change monotonically with temperature but should have a maximum value at a temperature, T_p , given by

$$T_p = \frac{\ln(c/a)}{h}. (10)$$

The Curie temperature is shown in Fig. 9 for Pd₇₇Cu₆Si₁₇, displaying a peak at $T_p = 1359 \pm 156$ K.

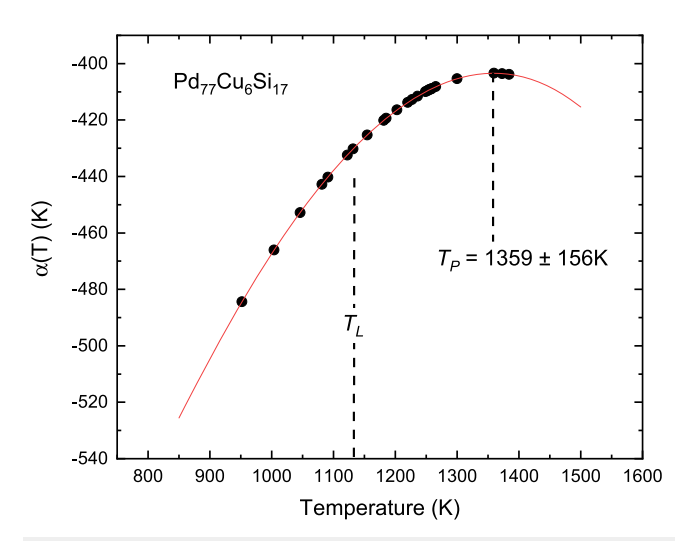


FIG. 9. The effective Curie temperature for liquid $Pd_{77}Cu_6Si_{17}$ over the temperature range that experimental x-ray diffraction data were collected. The liquidus temperature ($T_L = 1128$ K) is shown for reference.

TABLE III. Parameters obtained by fitting to the measured $S(q_1)$ as a function of temperature in liquid $Pd_{77}Cu_6Si_{17}$.

Parameter	Value	Uncertainty	% Uncertainty	Units
a	4.5	0.1	2.2	•••
b	-1.1×10^{-3}	0.1×10^{-3}	9	1/K
c	1.0	0.1	10	
T_{p}	1359	156	8.4	K

The parameters obtained by fitting Eq. (8) to the $S(q_1)$ data as a function of temperature for $Pd_{77}Cu_6Si_{17}$ are listed in Table III.

It follows naturally to consider whether a similar order parameter analysis of real-space quantities might elucidate more information about a transition from high temperature to low temperature behavior. Some fundamental work from the Yavari and co-workers5 identified inflections or crossovers in both the structure factors and pair-distribution functions in Pd- and Zr- based metallic glass forming liquids. Our analysis of the pair-distribution functions in Pd77Cu6Si17 did not find conclusive evidence for a crossover in the temperature dependence in any peak or peak location, owing mainly to large statistical uncertainties in the data obtained from a Fourier transform of the scattering data. Ideally, it would be useful to investigate the detailed structural ordering in a liquid obtained from a molecular dynamics simulation. Unfortunately, the one existing atomic potential was developed from experimental data that were taken in a contained environment and is thus not suitable for an MD analysis. A refinement of the potential using the higher quality data shown in Fig. 7 would allow for a quantitative comparison of the experimental data to the results of an MD simulation.

It is worth noting that for the Pd₇₇Cu₆Si₁₇ liquid, the effective Curie temperature (1359 \pm 156 K) is higher than the crossover between the high temperature and low temperature data observed in Fig. 8(a). Given the substantial uncertainty in T_p and the lack of any physically meaningful way to limit the temperature ranges fit for the "high temperature" and "low temperature" regimes, this is not surprising. The value of T_p is, however, consistent with values of the crossover temperature, T_A , measured from viscosity data of liquid Pd₇₇Cu₆Si₁₇ droplets.⁵⁴ While the temperature dependence of the shear viscosity for strong liquids, such as SiO2, is approximately Arrhenius from above the liquidus temperature to the glass transition temperature, metallic liquids show a crossover with decreasing temperature to a super-Arrhenius behavior (i.e., temperature dependent activation energy) beginning at a temperature T_A , located near the liquidus temperature. Molecular dynamics simulations suggest that the crossover is due to the onset of a cooperative response to local atomic excitations. 55,56 Above T_A , the characteristic time for the shear viscosity, called the Maxwell time, $\tau_{\rm M}$, is equal to the time required for an atomic cluster to gain or lose a single atom, τ_{LC} . At temperatures below T_A , τ_M becomes larger than τ_{LC} due to the increasing atomic cooperativity over increasingly larger length scales. Recent studies in another metallic glass forming system, Cu₄₉Zr₄₅Al₆, demonstrated that an observed peak in the effective Curie temperature occurred near the temperature of the breakdown of the Stokes-Einstein relation. The breakdown in

the cause of CuZrAl manifested as a rapid reduction in the relative diffusion coefficients between Cu, Zr, and Al.

Some studies suggest that glass formation occurs because of a frustration between the local order in the liquid and that required for crystallization. Drawing an analogy between frustration in coupled spin systems and liquids, Chakrabarty argued that the structure factor should show a Curie-Weiss behavior,⁵⁷ supported by a recent MD study that examined the order parameter defined in Eq. (7) ⁴⁹ The authors found that as predicted, $1/(S(T,q_1)-1)$ has a Curie-Weiss behavior with a negative Curie temperature, presumably reflecting the frustration. We suspect that the structural units that constitute the liquid will show distinct features connected to this onset, and we further suspect that glass forming ability is also distinguishable in the evolution of these structural features. Unfortunately, the embedded atom and angular dependent potentials are simply not accurate enough for these investigations to be made in Au-Si, Pd-Si, and Pd-Cu-Si. The potentials should be refined by comparison with the experimentally determined structure factors and pair-distribution functions in this work. Further progress on understanding the nature of the transition between high temperature and low temperature structural behavior in these liquids is hampered until the potentials are improved.

V. CONCLUSIONS

In summary, the total structure factor, S(q), and the pair-distribution function, g(r), obtained from experimental x-ray scattering data for equilibrium and supercooled $Au_{81}Si_{18}$, $Pd_{82}Si_{18}$, and $Pd_{77}Cu_6Si_{19}$ glass forming liquids, are presented. Some features of these quantities are similar to those observed in other metallic liquids. For example, the primary peak intensities in S(q) increase and shift to higher-q values with decreasing temperature, consistent with an increasing atomic density. However, a developing shoulder on the second peak of S(q) with decreasing temperature, which is commonly observed and attributed to local ordering in the liquid, is not present for the $Au_{81}Si_{18}$ liquid. This suggests significantly different ordering in this liquid.

The experimental S(q) data for the $Pd_{77}Cu_6Si_{17}$ liquid follow a Curie-Weiss behavior with a negative Curie temperature, as has been observed in a previous experimental study of a Pd_{42.5}Ni_{7.5}Cu₃₀P₂₀ glass forming liquid and from molecular dynamics (MD) simulations. The first peak in S(q) shows a non-linear behavior with decreasing temperature as we have observed in previous experimental studies of other metallic liquids. The effective Curie temperature obtained from the experimental scattering data goes through maximum at a temperature that is approximately the same as a dynamical crossover temperature in the viscosity, T_A , which corresponds to the onset of a cooperative response to local structural excitations, based on MD simulations. Recent studies also suggest that this is the temperature at which the Stokes-Einstein relation between the liquid viscosity and the diffusion coefficient begins to fail. The correlation between changes in S(q) and in the viscosity observed in the experimental data supports a connection between liquid structure and liquid dynamics, as has been previously argued.

Using an existing EAM potential for $Pd_{82}Si_{18}$ and an ADP potential for $Au_{81}Si_{18}$, S(q) and g(r) were calculated from classical MD simulations and compared with the experimental data. Only

qualitative agreement is observed with particularly poor agreement found for the $Au_{81}Si_{18}$ liquid. A Voronoi polyhedral analysis of the MD structures gives a broad distribution of cluster types in contradiction with the results of *ab initio* MD calculations. These points of disagreement demonstrate that the existing EAM and ADP potentials are incapable of accurately representing the atomic interactions and must be refined.

SUPPLEMENTARY MATERIAL

See the supplementary material for the figures that demonstrate that the MD simulations are sufficiently equilibrated and the figures that compare the structural data at all temperatures for the MD simulations and the experimental data.

ACKNOWLEDGMENTS

The authors thank Doug Robinson for his assistance with the high-energy x-ray diffraction studies at the APS. The work at St. Norbert College was supported by the National Science Foundation under Grants Nos. DMR-19-04466 and S-STEM-19-30274. The work at Washington University in Saint Louis was partially supported by the National Science Foundation under Grant No. DMR-19-04281. The synchrotron measurements were made on the Sector 6 beamline at the APS. The use of the APS is supported by the US Department of Energy, Basic Energy Science, Office of Science, under Contract No. DE-AC02-06CH11357. Any opinions, findings, and conclusions or recommendations expressed in this material are those of the author(s) and do not necessarily reflect the views of the National Science Foundation.

AUTHOR DECLARATIONS

Conflict of Interest

The authors have no conflicts to disclose.

Author Contributions

F.Z.C. and K.F.K. conducted all MD simulations in this study. N.A.M., K.F.K., and A.J.V. acquired experimental data for this work. N.A.M., K.R., C.U., S.M.B., and A.J.V. conducted analysis on the experimental data or the MD simulations. All authors contributed to the production of the manuscript.

F. Z. Chen: Data curation (equal); Formal analysis (equal); Investigation (equal); Methodology (equal); Software (equal); Writing – review & editing (equal). K. Ruhland: Formal analysis (equal); Software (equal); Writing – original draft (equal); Writing – review & editing (equal). C. Umland: Formal analysis (equal); Software (equal); Writing – original draft (equal); Writing – review & editing (equal). S. M. Bertrand: Formal analysis (equal); Software (equal); Writing – review & editing (equal). A. J. Vogt: Conceptualization (equal); Data curation (equal); Formal analysis (equal); Investigation (equal); Software (equal); Writing – review & editing (equal). K. F. Kelton: Conceptualization (equal); Data curation (equal); Formal analysis (equal); Funding acquisition (equal); Investigation (equal); Methodology (equal); Project administration (equal); Resources (equal); Software (equal); Supervision (equal); Validation (equal); Visualization (equal); Writing – original draft (equal);

Writing – review & editing (equal). N. A. Mauro: Conceptualization (equal); Data curation (equal); Formal analysis (equal); Funding acquisition (equal); Investigation (equal); Methodology (equal); Project administration (equal); Resources (equal); Software (equal); Supervision (equal); Validation (equal); Visualization (equal); Writing – original draft (equal); Writing – review & editing (equal).

DATA AVAILABILITY

The data that support the findings of this study are available from the corresponding author upon reasonable request.

REFERENCES

- W. Klement, R. H. Willens, and P. Duwez, "Non-crystalline structure in solidified gold-silicon alloys," Nature 187, 869–870 (1960).
 N. Jakse, T. L. T. Nguyen, and A. Pasturel, "Local order and dynamic properties
- 2 N. Jakse, T. L. T. Nguyen, and A. Pasturel, "Local order and dynamic properties of liquid $Au_x Si_{1-x}$ alloys by molecular dynamics simulations," J. Chem. Phys. 137, 204504 (2012).
- ³ A. Pasturel, E. S. Tasci, M. H. F. Sluiter, and N. Jakse, "Structural and dynamic evolution in liquid Au-Si eutectic alloy by *ab initio* molecular dynamics," Phys. Rev. B **81**, 140202 (2010).
- ⁴J. Schroers, B. Lohwongwatana, W. L. Johnson, and A. Peker, "Gold based bulk metallic glass," Appl. Phys. Lett. **87**, 061912 (2005).
- ⁵Y. Ke-Fu and R. Fang, "Pd-Si binary bulk metallic glass prepared at low cooling rate," Chin. Phys. Lett. **22**, 1481–1483 (2005).
- ⁶L. Liu, A. Inoue, and T. Zhang, "Formation of bulk Pd-Cu-Si-P glass with good mechanical properties," Mater. Trans. **46**, 376–378 (2005).
- ⁷Y. Q. Cheng and E. Ma, "Atomic-level structure and structure-property relationship in metallic glasses," Prog. Mater. Sci. **56**, 379 (2011).
- ⁸N. A. Mauro, M. Blodgett, M. L. Johnson, A. J. Vogt, and K. F. Kelton, "A structural signature of liquid fragility," Nat. Commun. 5, 4616 (2014).
- ⁹K. F. Kelton, G. W. Lee, A. K. Gangopadhyay, R. W. Hyers, T. J. Rathz, J. R. Rogers, M. B. Robinson, and D. S. Robinson, "First X-ray scattering studies on electrostatically levitated metallic liquids: Demonstrated influence of local icosahedral order on the nucleation barrier," Phys. Rev. Lett. 90, 195504 (2003).
- ¹⁰ K. F. Yao, F. Ruan, Y. Q. Yang, and N. Chen, "Superductile bulk metallic glass," Appl. Phys. Lett. 88, 122106 (2006).
- 11°C. W. Ryu and T. Egami, "Medium-range atomic correlation in simple liquids. I. Distinction from short-range order," Phys. Rev. E **104**, 064109 (2021).
- ¹²T. Egami and C. W. Ryu, "Structural principles in liquids and glasses: Bottom-up or top-down," Front. Mater. 9, 874191 (2022).
- 1³Y. Q. Cheng, J. Ding, and E. Ma, "Local topology vs. atomic-level stresses as a measure of disorder," Correlating Struct. Indic. Met. Glasses 1, 3–12 (2013).
- ¹⁴N. A. Mauro, V. Wessels, J. C. Bendert, S. Klein, A. K. Gangopadhyay, M. J. Kramer, S. G. Hao, G. E. Rustan, A. Kreyssig, A. I. Goldman, and K. F. Kelton, "Short- and medium-range order in Zr₈₀Pt₂₀ liquids," Phys. Rev. B 83, 184109 (2011).
- ¹⁵N. A. Mauro, W. Fu, J. C. Bendert, Y. Q. Cheng, E. Ma, and K. F. Kelton, "Local atomic structure in equilibrium and supercooled liquid Zr_{75.5}Pd_{24.5}," J. Chem. Phys. **137**, 044501 (2012).
- ¹⁶J. Maldonis, "Local structure analysis of model metal-metal and metal-metalloid metallic glasses," Ph.D. dissertation, University of Wisconsin–Madison, (2019).
- ¹⁷J. L. Finney, "Modelling the structures of amorphous metals and alloys," Nature **266**, 309–314 (1977).
- ¹⁸G. Guo, "Quasi-icosahedral clusters in Zr-based metallic glasses," Metals 10, 1135 (2020).
- ¹⁹ Z. J. Yang, L. Tang, T. Q. Wen, K. M. Ho, and C. Z. Wang, "Effects of Si solute on the glass formation and atomic structure of Pd liquid," J. Phys.: Condens. Matter **31**, 135701 (2019).
- ²⁰M. Durandurdu, "Ab initio modeling of metallic Pd₈₀Si₂₀ glass," Comput. Mater. Sci. 65, 44–47 (2012).

- ²¹ H. B. Lou, L. H. Xiong, A. S. Ahmad, A. G. Li, K. Yang, K. Glazyrin, H. P. Liermann, H. Franz, X. D. Wang, Q. P. Cao, D. X. Zhang, and J. Z. Jiang, "Atomic structure of Pd₈₁Si₁₉ glassy alloy under high pressure," Acta Mater. **81**, 420–427 (2014).
- ²²N. A. Mauro and K. F. Kelton, "A highly modular beamline electrostatic levitation facility, optimized for in situ high-energy x-ray scattering studies of equilibrium and supercooled liquids," Rev. Sci. Instrum. **82**, 035114–035119 (2011).
- ²³ H. W. Kui, A. L. Greer, and D. Turnbull, "Formation of bulk metallic glass by fluxing," Appl Phys. Lett. 45, 615–616 (1984).
- ²⁴J. C. Bendert, C. E. Pueblo, S. Veligati, N. A. Mauro, and K. F. Kelton, "Temperature calibration for optical pyrometry in containerless systems using differential scanning calorimetry: Application to $Cu_{100-x}Zr_x$, (x=45-50)," Int. J. Thermophys. 35, 1687–1696 (2014).
- ²⁵S. K. Chung, D. B. Thiessen, and W. K. Rhim, "A noncontact measurement technique for the density and thermal expansion coefficient of solid and liquid materials," Rev. Sci. Instrum. **67**, 3175–3181 (1996).
- ²⁶R. C. Bradshaw, D. P. Schmidt, J. R. Rogers, K. F. Kelton, and R. W. Hyers, "Machine vision for high-precision volume measurement applied to levitated containerless material processing," Rev. Sci. Instrum. 76, 125108 (2005).
- ²⁷P. F. Peterson, E. S. Božin, T. Proffen, and S. J. L. Billinge, "Improved measures of quality for the atomic pair distribution function," J. Appl. Crystallogr. **36**, 53–64 (2003).
- ²⁸F. Z. Chen, N. A. Mauro, S. M. Bertrand, P. McGrath, L. Zimmer, and K. F. Kelton, "Breakdown of the Stokes–Einstein relationship and rapid structural ordering in CuZrAl metallic glass-forming liquids," J. Chem. Phys. 155, 104501 (2021).
- ²⁹ M. L. Johnson, M. E. Blodgett, K. A. Lokshin, N. A. Mauro, J. Neuefeind, C. Pueblo, D. G. Quirinale, A. J. Vogt, T. Egami, A. I. Goldman, and K. F. Kelton, "Measurements of structural and chemical order in Zr₈₀Pt₂₀ and Zr₇₇Rh₂₃," Phys. Rev. B **93**, 054203 (2016).
- ³⁰ A. P. Hammersley, S. O. Svensson, M. Hanfland, A. N. Fitch, and D. Hausermann, "Two-dimensional detector software: From real detector to idealised image or two-theta scan," Int. J. High Pressure Res. **14**, 235–248 (1996)
- ³¹ J. Towns, T. Cockerill, M. Dahan, I. Foster, K. Gaither, A. Grimshaw, V. Hazlewood, S. Lathrop, D. Lifka, and G. D. Peterson, "XSEDE: Accelerating scientific discovery," Comput. Sci. Eng. 16, 62–74 (2014).
- ³²H. W. Sheng, M. J. Kramer, A. Cadien, T. Fujita, and M. W. Chen, "Highly optimized embedded-atom-method potentials for fourteen fcc metals," Phys. Rev. B 83, 134118 (2011).
- ³³M. J. K. H. Sheng, "Atomic structure and dynamics of Pd-Si metallic glass" (unpublished) (2022).
- ³⁴S. V. Starikov, N. Y. Lopanitsyna, D. E. Smirnova, and S. V. Makarov, "Atomistic simulation of Si-Au melt crystallization with novel interatomic potential," Comput. Mater. Sci. **142**, 303–311 (2018).
- ³⁵T. E. Faber and J. M. Ziman, "A theory of the electrical properties of liquid metals," Philos. Mag. 11, 153–173 (1965).
- ³⁶G. W. Lee, A. K. Gangopadhyay, K. F. Kelton, R. W. Hyers, T. J. Rathz, J. R. Rogers, and D. S. Robinson, "Difference in icosahedral short-range order in early and late transition metal liquids," Phys. Rev. Lett. 93, 037802 (2004).
- ³⁷H. Okamoto, "Pd-Si (Palladium-Silicon)," J. Phase Equilib. **14**, 536–538 (1993).
- ³⁸Y. Li, "A relationship between glass-forming ability and reduced glass transition temperature near eutectic composition," Mater. Trans. **42**, 556–561 (2001).

- ³⁹S. Pan, J. Qin, W. Wang, and T. Gu, "Origin of splitting of the second peak in the pair-distribution function for metallic glasses," Phys. Rev. B **84**, 092201 (2011).
- ⁴⁰ J. D. Honeycutt and H. C. Andersen, "Molecular dynamics study of melting and freezing of small Lennard-Jones clusters," J. Phys. Chem. **91**, 4950–4963 (1987).
- ⁴¹P. J. Steinhardt, D. R. Nelson, and M. Ronchetti, "Bond-orientational order in liquids and glasses," Phys. Rev. B **28**, 784–805 (1983).
- ⁴²A. Stukowski, "Visualization and analysis of atomistic simulation data with OVITO-the open visualization tool," Modell. Simul. Mater. Sci. Eng. 18, 015012 (2009).
- 43 F. Dong, G. Q. Yue, Y. R. Guo, C. Qiao, Z. Y. Wang, Y. X. Zheng, R. J. Zhang, Y. Sun, W. S. Su, and M. J. Kramer, "Si-centered capped trigonal prism ordering in liquid Pd₈₂ Si₁₈ alloy study by first-principles calculations," RSC Adv. 7, 18093–18098 (2017).
- ⁴⁴L. Yang and G.-Q. Guo, "Preferred clusters in metallic glasses," Chin. Phys. B 19, 126101 (2010).
- 45 M. Li, C. Z. Wang, S. G. Hao, M. J. Kramer, and K. M. Ho, "Structural heterogeneity and medium-range order in Zr_xCu_{100-x} metallic glasses," Phys. Rev. B **80**, 184201 (2009).
- ⁴⁶T. Fujita, K. Konno, W. Zhang, V. Kumar, M. Matsuura, A. Inoue, T. Sakurai, and M. W. Chen, "Atomic-scale heterogeneity of a multicomponent bulk metallic glass with excellent glass forming ability," Phys. Rev. Lett. **103**, 075502 (2009).
- ⁴⁷L. Yang, G. Q. Guo, L. Y. Chen, C. L. Huang, T. Ge, D. Chen, P. K. Liaw, K. Saksl, Y. Ren, Q. S. Zeng, B. LaQua, F. G. Chen, and J. Z. Jiang, "Atomic-scale mechanisms of the glass-forming ability in metallic glasses," Phys. Rev. Lett. 109, 105502 (2012).
- ⁴⁸J. Finney, "Random packings and the structure of simple liquids. I. The geometry of random close packing," Proc. R. Soc. London, Ser. A **319**, 479–493 (1970).
- ⁴⁹C. W. Ryu, W. Dmowski, K. F. Kelton, G. W. Lee, E. S. Park, J. R. Morris, and T. Egami, "Curie-Weiss behavior of liquid structure and ideal glass state," Sci. Rep. **9**, 18579 (2019).
- 50 H. S. Chen and B. K. Park, "Role of chemical bonding in metallic glasses," Acta Metall. **21**, 395–400 (1973).
- 51 G. Q. Yue, Y. Zhang, Y. Sun, B. Shen, F. Dong, Z. Y. Wang, R. J. Zhang, Y. X. Zheng, M. J. Kramer, and S. Y. Wang, "Local structure order in $Pd_{78}Cu_6Si_{16}$ liquid," Sci. Rep. 5, 8277 (2015).
- ⁵² K. Georgarakis, L. Hennet, G. A. Evangelakis, J. Antonowicz, G. B. Bokas, V. Honkimaki, A. Bytchkov, M. W. Chen, and A. R. Yavari, "Probing the structure of a liquid metal during vitrification," Acta Mater. 87, 174–186 (2015).
- ⁵³D. V. Louzguine-Luzgin, R. Belosludov, A. R. Yavari, K. Georgarakis, G. Vaughan, Y. Kawazoe, T. Egami, and A. Inoue, "Structural basis for supercooled liquid fragility established by synchrotron-radiation method and computer simulation," J. Appl. Phys. 110, 043519 (2011).
- ⁵⁴M. D. Demetriou, J. S. Harmon, M. Tao, G. Duan, K. Samwer, and W. L. Johnson, "Cooperative shear model for the rheology of glass-forming metallic liquids," Phys. Rev. Lett. **97**, 065502 (2006).
- 55T. Iwashita, D. M. Nicholson, and T. Egami, "Elementary excitations and crossover phenomenon in liquids," Phys. Rev. Lett. 110, 205504 (2013).
- ⁵⁶R. Soklaski, V. Tran, Z. Nussinov, K. F. Kelton, and L. Yang, "A locally preferred structure characterises all dynamical regimes of a supercooled liquid," Philos. Mag. 96, 1212–1227 (2016).
- ⁵⁷S. Chakrabarty and Z. Nussinov, "High-temperature correlation functions: Universality, extraction of exchange interactions, divergent correlation lengths, and generalized Debye length scales," Phys. Rev. B 84, 064124 (2011).